Brain, Behavior, and Immunity 140 (2027) 107082

Contents lists available at ScienceDirect

Brain Behavior and Immunity

journal homepage: www.elsevier.com/locate/ybrbi

Full-length Article

Persistent microbial-derived material accumulates after brain injury and associates with chronic neuroinflammation

Hongmei Yang [a], Olivia Shyong [a], Limin Wu [a], Evan C. Marcet [b], Brianne E. Dillon [a], Jaina T. Dillon [a], Dalila M. Marzialo [a], Aubrienne Krysiewicz-Bell [a], Lindsay E. Popeo [a], Shirin Jamali [a], Graham Y. Schrodel [a], Amir Davis [a], Aria Shi [a], Dana M. Cairns [b], Liam H. Power [b], David L. Kaplan [b], Ann McKee [c], Daniel H. Daneshvar [c], Mariana Vinacur [d], Gerald B. Pier [d], Ross Zafonte [e,***], Michael J. Whalen [a,**], Colette Cywes-Bentley [d,*]

[a] Department of Pediatrics, Massachusetts General Hospital and Harvard Medical School, Boston, MA 02114, USA
[b] Department of Biomedical Engineering, Tufts University, Medford, MA 02155, USA
[c] Department of Neurology and Pathology, Boston University Alzheimer's Disease Research Center and Chronic Traumatic Encephalopathy Center, Chobanian and Avedisian School of Medicine, Boston, MA 02118, USA
[d] Division of Infectious Diseases, Department of Medicine, Brigham and Women's Hospital, Harvard Medical School, Boston, MA 02115, USA
[e] University of Missouri School of Medicine, Columbia, MO 65212, USA

ARTICLE INFO

Keywords:
Traumatic brain injury
Chronic traumatic encephalopathy
Neuroinflammation
Microbiome-brain axis
Poly-*N*-acetyl-glucosamine (PNAG)
Tau phosphorylation
Microglia
Persistent microbial material

ABSTRACT

Objective: Traumatic brain injury (TBI) is associated with chronic neurodegenerative sequelae, including chronic traumatic encephalopathy (CTE), but mechanisms sustaining long-term neuroinflammation in the injured brain remain unclear. Persistent, poorly cleared biological material has been proposed as a driver of chronic inflammation. This study tested whether microbial-derived material is present in CTE and experimental brain injury, and whether reducing such material is associated with improved outcomes.

Methods: Post-mortem brain tissue from individuals with CTE and controls was analyzed for the microbial polysaccharide poly-*N*-acetyl-glucosamine (PNAG) and phosphorylated tau (pTau). Mice were subjected to single and repetitive closed head injury (CHI), with assessment of brain PNAG and tau accumulation, behavior, and neuropathology. Purified PNAG was administered intracerebrally to evaluate biological effects. Passive antibody treatment and active vaccination targeting PNAG were used to determine whether reducing brain PNAG altered outcomes after CHI.

Results: PNAG accumulated in human CTE brains in a disease stage-dependent manner and colocalized with pTau. In mice, PNAG rapidly accumulated across multiple brain regions after CHI and remained elevated at two weeks. Intracerebral administration of purified PNAG induced physiological and behavioral deficits that differed by sex, whereas a lower dose produced no detectable behavioral deficits. Passive anti-PNAG antibody treatment reduced brain PNAG with limited functional benefit, whereas active vaccination in adolescence and early adulthood reduced brain PNAG accumulation and IBA1 immunoreactivity, was associated with lower pTau accumulation, and improved long-term motor outcomes one year after repetitive CHI.

Conclusions: Persistent microbial-derived material is detectable in human CTE and experimental TBI. Reduction of PNAG-associated microbial-derived material is associated with attenuation of chronic neuroinflammation, pathological tau accumulation, and improved long-term neurological outcomes, supporting a model in which persistent microbial-derived material may contribute to chronic post-traumatic neuroinflammation.

* Correspondence author at: Division of Infectious Diseases, Department of Medicine, Brigham and Women's Hospital, Harvard Medical School, 181 Longwood Ave, Boston, MA 02115, USA.
** Corresponding author at: Department of Pediatrics, Massachusetts General Hospital and Harvard Medical School, 55 Fruit St, Boston, MA, 02114, USA.
*** Corresponding author at: University of Missouri School of Medicine, Columbia, Missouri 65212, USA.
E-mail addresses: rzbg3@health.missouri.edu (R. Zafonte), mwhalen@mgh.harvard.edu (M.J. Whalen), ccywesbentley@bwh.harvard.edu (C. Cywes-Bentley).

https://doi.org/10.1016/j.bbi.2026.107082
Received 28 May 2026; Received in revised form 7 October 2026; Accepted 21 October 2026
Available online 25 October 2026
0889-1591/© 2026 Published by Elsevier Inc.

1. Introduction

Traumatic brain injury (TBI) initiates neuroinflammatory responses that can persist long after the initial insult and are associated with an increased risk of chronic neurodegenerative conditions, including chronic traumatic encephalopathy (CTE) (Brett et al., 2022; Bieniek et al., 2021). While acute inflammatory signaling after TBI is well characterized, the substrates that sustain chronic neuroinflammation remain incompletely defined. One emerging concept is that persistent microbial-derived material may serve as a long-lived stimulus that maintains immune activation and promotes progressive tissue dysfunction.

In peripheral tissues, microbial-derived products can persist and drive chronic inflammation when clearance mechanisms are insufficient. In the central nervous system, this effect may be amplified, as immune surveillance and degradative pathways are more constrained, and mammals lack enzymatic pathways for degradation of certain microbial polymers. Traumatic brain injury is also associated with systemic changes, including increased gut permeability and release of microbial products into circulation, raising the possibility that microbial-derived material may accumulate in the brain following injury and contribute to sustained neuroimmune activation (Yuan et al., 2021; Oyovwi and Udi, 2025). However, whether such material is detectable within brain tissue after injury and whether it is associated with pathological outcomes remain largely unexplored.

Poly-*N*-acetyl-glucosamine (PNAG) is a conserved surface polysaccharide expressed by a wide range of bacteria, fungi, and other microorganisms, including members of the microbiota (Cywes-Bentley et al., 2013; Maira-Litrán et al., 2005; Gening et al., 2020). It is a major component of microbial biofilms and extracellular vesicles and is known to activate innate and adaptive immune responses. Because mammals lack enzymes capable of degrading this polymer, PNAG represents a candidate example of a persistent microbial-derived substrate that could accumulate in tissues and sustain inflammatory signaling. In this study, we used PNAG as a molecular tracer for microbial-derived material and as a targetable substrate to examine its potential role in post-traumatic neuroinflammation.

We hypothesized that microbial-derived material accumulates in the brain after injury and is associated with neuroinflammatory and neurodegenerative markers, and that reducing this material may modify post-injury outcomes. To test this, we examined post-mortem brain tissue from individuals with chronic traumatic encephalopathy for the presence of PNAG and its relationship to pTau. We then used mouse models of single and repetitive closed head injury to assess the temporal accumulation and distribution of PNAG in the brain. To evaluate biological plausibility, we examined the effects of intracerebral exposure to purified PNAG on physiological and behavioral outcomes. Finally, we used passive antibody treatment and active vaccination approaches targeting PNAG to determine whether reducing microbial-derived material in the injured brain is associated with changes in neuroinflammation, pTau accumulation, and long-term neurological function.

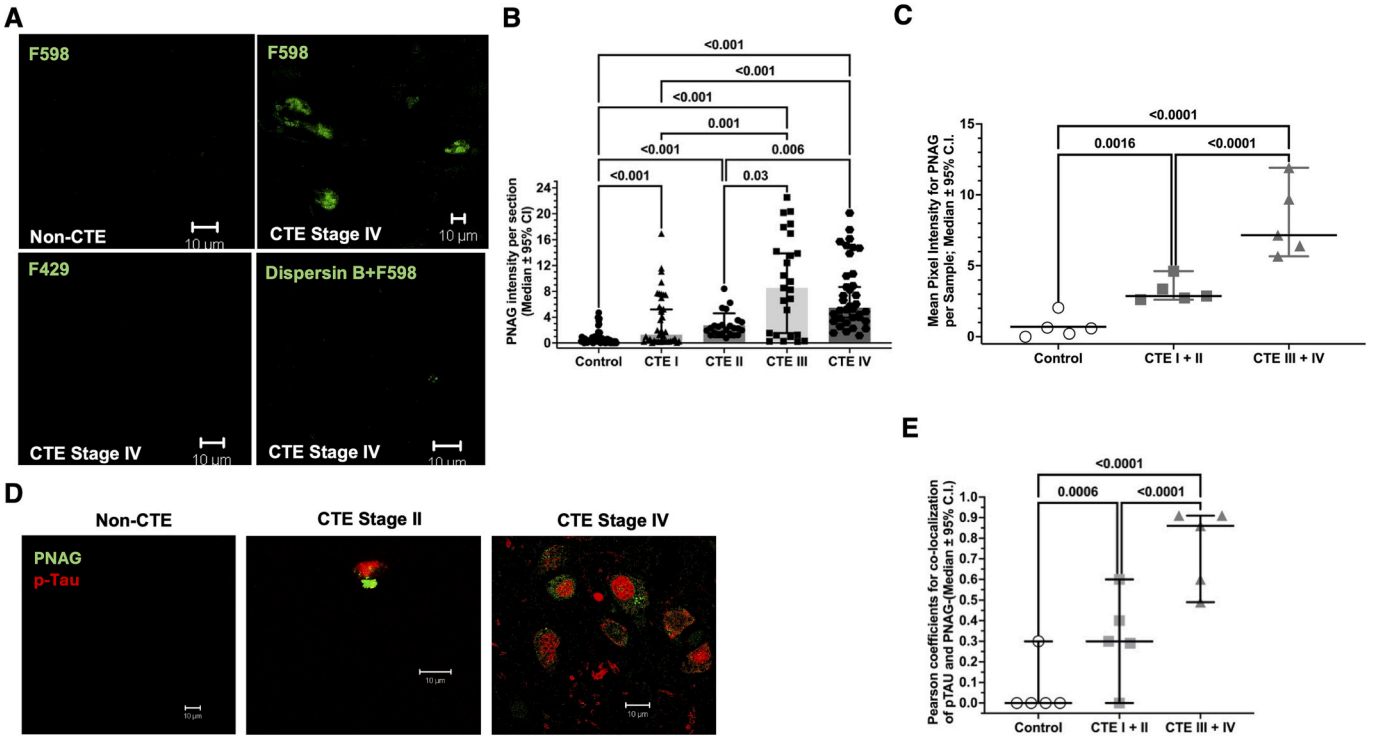


Fig. 1. PNAG accumulates progressively during human CTE and colocalizes with pTau. (A) Representative confocal images of PNAG immunostaining in non-CTE control and CTE brain tissue using the PNAG-specific monoclonal antibody F598 or the isotype control antibody F429. Enzymatic digestion with Dispersin B abolished PNAG immunoreactivity, confirming staining specificity. Scale bar, 10 µm. (B) Quantification of PNAG mean fluorescence intensity (MFI) in all individual tissue sections. Kruskal–Wallis test, overall $P < 0.001$. Pairwise comparisons shown on the graph were adjusted using the two-stage linear step-up procedure of Benjamini, Krieger and Yekutieli; q values are shown. Non-CTE controls, n = 5; stage I, n = 3; stage II, n = 2; stage III, n = 2; stage IV, n = 3. (C) PNAG mean pixel intensity per individual sample stratified by CTE stage, presented as median ± 95% CI. Overall two-way ANOVA, $P < 0.0001$. Pairwise comparisons shown on the graph were adjusted using the two-stage linear step-up procedure of Benjamini, Krieger and Yekutieli; q values are shown. Non-CTE controls, n = 5; CTE subjects, n = 10. (D) Representative confocal images demonstrating colocalization of PNAG (green) with pTau (red). Scale bar, 10 µm. (E) Quantification of PNAG–pTau colocalization using Pearson correlation coefficients, presented as median ± 95% CI. Overall two-way ANOVA, $P < 0.0001$. Pairwise comparisons shown on the graph were adjusted using the two-stage linear step-up procedure of Benjamini, Krieger and Yekutieli; q values are shown. Non-CTE controls, n = 5; CTE subjects, n = 10.

2. Results

2.1. Microbial-derived material accumulates progressively during human CTE and associates with phosphorylated tau

PNAG, used here as a tracer and experimentally tractable representative of microbial-derived material, showed minimal immunoreactivity in non-CTE control brain tissue, comparable to isotype control staining, whereas robust signal was detected in CTE samples. Enzymatic digestion with Dispersin B abolished PNAG immunoreactivity, supporting the specificity of PNAG staining (Fig. 1A). Quantitative analysis demonstrated significantly increased PNAG mean fluorescence intensity (MFI) in CTE compared with controls (Kruskal–Wallis test, $P < 0.001$; Fig. 1B). Stratification by disease stage further demonstrated progressive PNAG accumulation, with significantly higher levels in stage III/IV than stage I/II CTE, while both groups remained elevated relative to controls (Fig. 1C). PNAG frequently colocalized with pTau within regions of pathology (Fig. 1D). Quantification confirmed that PNAG–pTau colocalization increased progressively across disease stages (overall two-way ANOVA, $P < 0.0001$; Fig. 1E), consistent with an increasing association between microbial-derived material and tau pathology with advancing CTE stage.

2.2. Purified PNAG induces tau phosphorylation in human neural cells

Exposure of differentiated human neural stem cells and induced pluripotent stem cell (iPSC)-derived neurons to purified PNAG increased pTau compared with vehicle-treated controls (Fig. 2A). Specifically, PNAG-treated iPSC-derived neurons exhibited increased pTau (Ser202/Thr205; AT8) one week after exposure ($P < 0.0001$; Fig. 2B), while neural stem cells exhibited increased pTau (Thr181) two weeks after exposure ($P = 0.0158$; Fig. 2C). PNAG and pTau exhibited colocalization in treated cultures (Fig. 2A), supporting the biological plausibility that microbial-derived material can induce tau phosphorylation in human neural cells.

2.3. Microbial-derived material accumulates rapidly and persists for at least two weeks across multiple brain regions after closed head injury in mice

Following a single CHI, regional analysis demonstrated significantly increased PNAG accumulation in the cortex, hippocampus, and striatum at both 24 h and two weeks after injury compared with sham controls (Fig. 3A–B). PNAG colocalized with neurons and microglia but not astrocytes (Fig. 3C), and was detected in close proximity to pTau within injured, but not sham, brain tissue (Fig. 3D), consistent with the persistent accumulation of microbial-derived material in regions associated with neuroinflammation and neurodegeneration. Additional examples of PNAG colocalization with microglia and Aβ following repetitive CHI are shown in Supplementary Fig. S1.

2.4. Purified PNAG is sufficient to induce sex-dependent behavioral deficits in vivo

To determine whether purified microbial-derived material is sufficient to induce neurological dysfunction, PNAG was administered bilaterally into the striatum of male and female mice (Fig. 4A). PNAG administration resulted in reduced body weight in both sexes compared with PBS-treated controls (repeated-measures ANOVA, overall group effect, $P < 0.0001$; Fig. 4B). Male mice exhibited significant motor deficits on the rotarod following PNAG administration, whereas comparable deficits were not detected in females (repeated-measures ANOVA, overall group effect, $P = 0.004$; Fig. 4C). Male mice demonstrated impaired spatial learning during Morris water maze hidden-platform testing following PNAG administration, whereas a significant difference was not detected in females (repeated-measures ANOVA, overall group effect, $P < 0.0001$; Fig. 4D). Performance during probe trials was not significantly different between groups (Fig. 4E). In the open field test, spontaneous locomotor activity was significantly reduced in male PNAG-treated mice compared with male PBS-treated controls ($q < 0.001$), whereas the corresponding difference in females did not reach significance ($q = 0.06$; overall one-way ANOVA, $P < 0.0001$; Fig. 4F). Together, these findings demonstrate that purified PNAG is sufficient to induce neurological dysfunction in vivo, with the pattern and magnitude of behavioral effects differing between males and females. In contrast, a lower dose of PNAG did not induce detectable behavioral deficits (Supplementary Fig. S2).

2.5. PNAG vaccination confers sustained long-term motor benefit after repetitive brain injury

PNAG vaccination elicited robust anti-PNAG antibody responses (Fig. 5B) without affecting body weight throughout the study period (Fig. 5C). In the Morris water maze, hidden-platform trials showed an overall group effect at one week after injury (repeated-measures ANOVA, $P = 0.0164$; Fig. 5D). PNAG-vaccinated injured mice differed significantly from sham animals ($P = 0.015$), whereas TT-vaccinated injured mice did not ($P = 0.0955$); the two injured groups did not

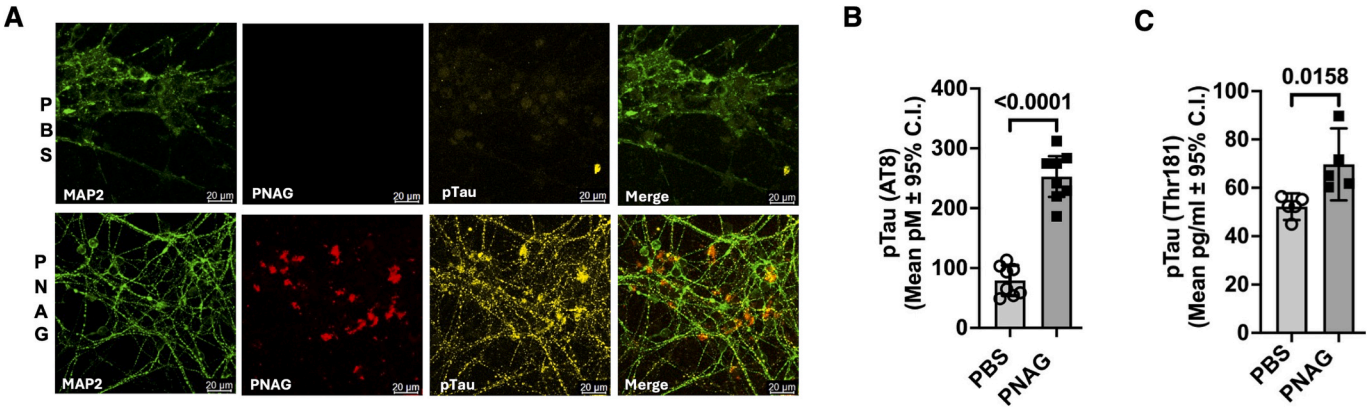


Fig. 2. Purified PNAG induces tau phosphorylation in human neural cell models. (A) Immunofluorescence images of human neural stem cells treated with PBS or PNAG showing colocalization of PNAG and pTau. Scale bar, 20 μm. (B) Quantification of tau phosphorylated at Ser202/Thr205 in human iPSC-derived neuron lysates by ELISA 1 week after treatment with PBS or PNAG (10 μg/mL). The *P* value is from a two-tailed *t*-test; n = 8/group. (C) Quantification of tau phosphorylated at Thr181 in human iNSC lysates by ELISA 2 weeks after treatment with PBS or PNAG (10 μg/mL). The *P* value is from a two-tailed *t*-test; n = 5/group. Data are from 3 to 5 independent experiments per condition.

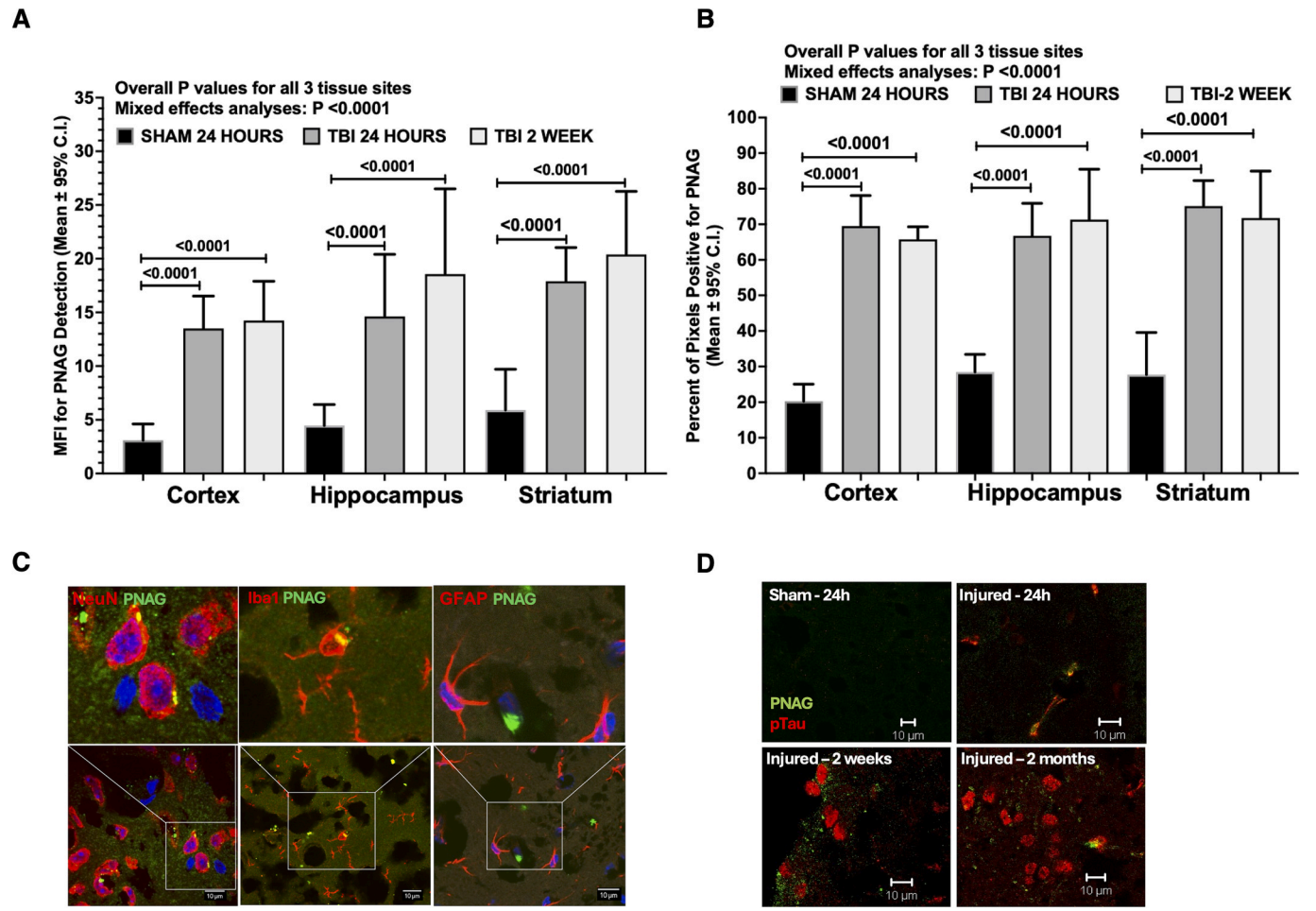


Fig. 3. PNAG rapidly accumulates and persists for at least two weeks after closed head injury in male mice. (A) Quantification of PNAG mean fluorescence intensity (MFI) in the cortex, hippocampus, and striatum at 24 h and 2 weeks following CHI compared with sham controls. (B) Quantification of the percentage of PNAG-positive pixels in the cortex, hippocampus, and striatum at 24 h and 2 weeks following CHI compared with sham controls. (C) Representative images showing PNAG colocalization with neurons (NeuN) and microglia (IBA1), but not astrocytes (GFAP), following CHI. (D) Representative images showing PNAG in close proximity to phosphorylated tau (pTau) in sham brain tissue at 24 h and injured brain tissue at 24 h, 2 weeks, and 2 months after CHI.

differ significantly from each other (P = 0.7236). At one year, hidden-platform trials showed an overall group effect (repeated-measures ANOVA, P = 0.0314; Fig. 5D). PNAG-vaccinated injured mice differed significantly from sham animals (P = 0.024), whereas TT-vaccinated injured mice did not (P = 0.4352); the two injured groups did not differ significantly from each other (P = 0.3496). No differences among groups were observed during visible-platform testing at any time point. Probe trial performance did not differ among groups at any time point (Fig. 5E). In contrast, PNAG vaccination produced sustained improvement in motor function on the rotarod (repeated-measures ANOVA, overall group effect, P = 0.0104; Fig. 5F). PNAG-vaccinated injured mice performed similarly to sham controls (P = 0.9235) and significantly better than TT-vaccinated injured mice (P = 0.0317), whereas TT-vaccinated injured mice exhibited significant motor deficits compared with sham controls (P = 0.0133). These findings indicate that PNAG vaccination provides sustained motor benefit following repetitive brain injury, while cognitive performance was not improved.

2.6. PNAG vaccination reduces persistent neuropathology one year after repetitive brain injury

One year after repetitive CHI, PNAG accumulation differed significantly among groups (one-way ANOVA, $P < 0.0001$; Fig. 6A–B), as did IBA1 immunoreactivity (one-way ANOVA, $P < 0.0001$; Fig. 6C–D) and pTau accumulation (Welch's ANOVA, $P = 0.0051$; Fig. 6E–F). PNAG vaccination significantly reduced PNAG accumulation and IBA1 immunoreactivity compared with control-vaccinated injured mice ($P < 0.0001$ for both comparisons). pTau accumulation was significantly lower in PNAG-vaccinated than in control-vaccinated injured mice ($P = 0.0134$); PNAG-vaccinated injured mice also differed significantly from sham animals ($P = 0.0048$), whereas control-vaccinated injured mice did not differ significantly from sham animals ($P = 0.1231$). Passive anti-PNAG antibody treatment also reduced brain PNAG accumulation but produced more limited behavioral effects than active vaccination (Supplementary Figs. S3–S4).

3. Discussion

Traumatic brain injury initiates neuroinflammatory responses that can persist long after the inciting event, yet the substrates that sustain this chronic inflammation remain incompletely defined. Here, we identify persistent microbial-derived material in post-mortem brain tissue from individuals with CTE and demonstrate that the microbial polysaccharide PNAG accumulates rapidly and persists after closed head injury in mice. Using complementary human tissue, in vitro, and in vivo experimental models, we further show that purified PNAG is sufficient to induce pathological tau phosphorylation and neurological dysfunction, whereas reducing PNAG through immunological approaches was associated with reduced brain PNAG accumulation, decreased IBA1 immunoreactivity, lower pTau accumulation, and improved long-term motor

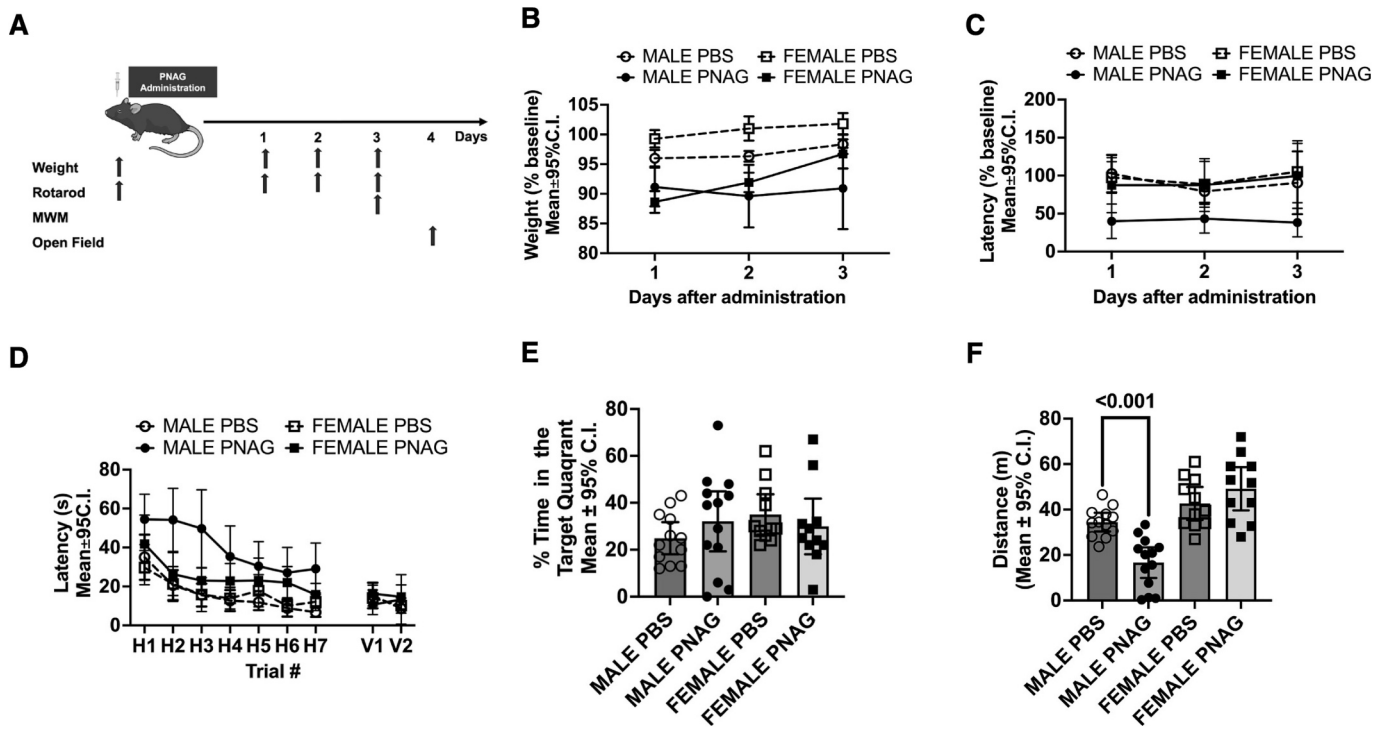


Fig. 4. Intrastriatal administration of purified PNAG induces sex-dependent behavioral deficits in male and female mice. (A) Experimental design for intrastriatal PNAG administration. (B) Body weight changes following PNAG or PBS injection. Repeated-measures ANOVA, overall group effect, $P < 0.0001$; sex × treatment interaction, $P = 0.002$. Tukey's multiple-comparisons test: male PBS vs. PNAG, $P = 0.0064$; female PBS vs. PNAG, $P = 0.0006$; female PNAG vs. male PNAG, $P = 0.7522$. n = 11–13 mice/group. (C) Rotarod performance following PNAG or PBS injection. Repeated-measures ANOVA, overall group effect, $P = 0.004$; sex × treatment interaction, $P = 0.183$. Tukey's multiple-comparisons test: male PBS vs. PNAG, $P = 0.0201$; female PBS vs. PNAG, $P = 0.9891$; female PNAG vs. male PNAG, $P = 0.0215$. n = 11–13 mice/group. (D) Morris water maze performance during hidden-platform trials. Repeated-measures ANOVA, overall group effect, $P < 0.0001$; sex × treatment interaction, $P = 0.0172$. Tukey's multiple-comparisons test: male PBS vs. PNAG, $P = 0.0002$; female PBS vs. PNAG, $P = 0.5064$; male PNAG vs. female PNAG, $P = 0.0339$. Visible-platform testing showed no significant overall group effect (repeated-measures ANOVA, $P = 0.52$). n = 11–13 mice/group. (E) Probe trial performance. One-way ANOVA, $P = 0.50$; n = 11–13 mice/group. (F) Open-field activity following PNAG administration. One-way ANOVA, overall group effect, $P < 0.0001$. Pairwise comparisons were adjusted using the two-stage linear step-up procedure of Benjamini, Krieger and Yekutieli: male PBS vs. PNAG, $q < 0.001$; female PBS vs. PNAG, $q = 0.06$; male PNAG vs. female PNAG, $q < 0.001$. Male PBS, n = 12; male PNAG, n = 13; female PBS, n = 11; female PNAG, n = 11.

outcomes. Together, these findings support a model in which persistent microbial-derived material may contribute to sustained neuroimmune activation following brain injury.

A central advance of this study is the direct identification of microbial-derived material within injured brain tissue. Prior work has largely focused on indirect effects of the gut microbiome on brain injury outcomes, including systemic immune activation, altered gut permeability, and circulating microbial metabolites (Shumilov et al., 2024; Gu et al., 2024). The relationship between TBI and the gut microbiome is bidirectional, with brain injury altering gut microbial composition and gut dysbiosis in turn influencing neuroinflammation and neurological outcomes. These effects may involve microbial metabolites and modulation of peripheral and central immune responses (Panther et al., 2022). In contrast, our findings suggest that microbial structural components are detectable within the brain parenchyma following injury and can persist long after the initial insult. In this study, PNAG served as a broadly expressed microbial polysaccharide that enabled us to trace and experimentally manipulate persistent microbial-derived material, rather than implicate a single molecular species as the sole driver of pathology. The rapid appearance of PNAG within the brain following CHI is consistent with entry from the systemic circulation, while its persistence at two weeks suggests limited clearance, although the precise trafficking and clearance mechanisms remain to be determined. Given the absence of known mammalian enzymes capable of degrading PNAG, this material may represent a durable immunostimulatory substrate within the injured brain, consistent with the capacity of bacterial membrane-derived material to exert sustained biological effects (Kim et al., 2017).

The human data demonstrate that PNAG accumulation increases with CTE stage and colocalizes with pTau in regions of pathology. While these observations establish association rather than causality, they define a spatial and disease-relevant relationship between persistent microbial-derived material and a hallmark of CTE pathology. Complementary in vitro experiments demonstrating tau phosphorylation following exposure to purified PNAG provide evidence of biological plausibility. However, the mechanisms linking PNAG to tau phosphorylation remain undefined and require further investigation.

The experimental models further support a functional contribution of persistent microbial-derived material to post-injury outcomes. Intracerebral administration of purified PNAG was sufficient to induce weight loss and neurological deficits, some of which were also observed following CHI; however, cellular and molecular features of CHI pathology were not evaluated in these experiments. Active immunization, and to a lesser extent passive antibody treatment, reduced PNAG accumulation in the injured brain. Active vaccination was also associated with reduced IBA1 immunoreactivity, lower pTau accumulation, and sustained improvement in long-term motor function. These findings support a model in which persistent microbial-derived material may contribute to chronic neuroinflammatory processes that influence long-term functional recovery following brain injury.

Notably, the effects of PNAG modulation were more consistent for motor outcomes than for cognitive measures. Although PNAG vaccination produced robust and durable improvements in motor function, it did not improve spatial learning; PNAG-vaccinated injured mice showed impaired hidden-platform performance relative to sham animals,

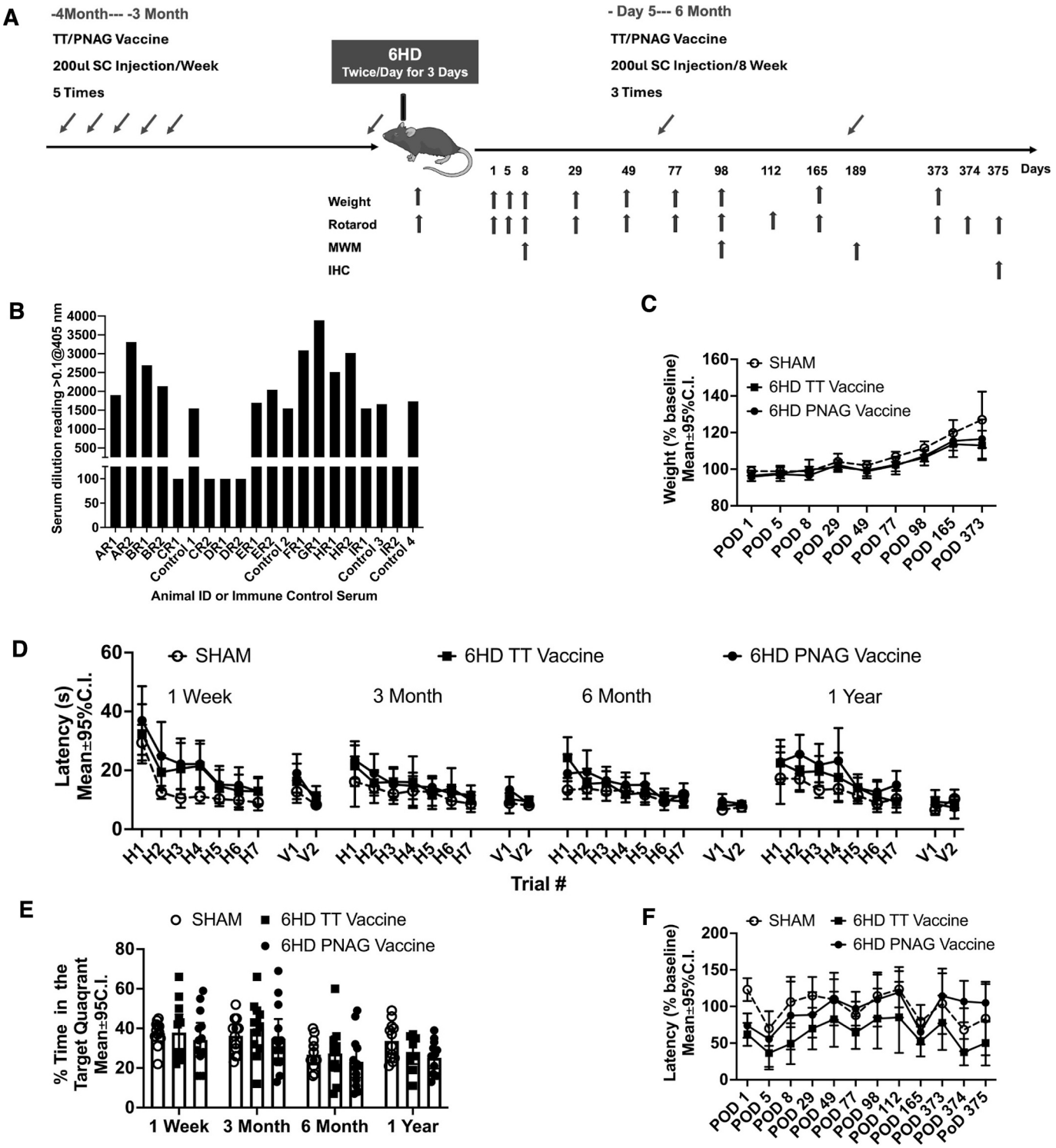


Fig. 5. Long-term functional outcomes: PNAG vaccination confers sustained motor benefit after repetitive brain injury in male mice. (A) Experimental design for long-term study. (B) Antibody titers following vaccination. Control samples represent a known immune mouse serum included to monitor plate-to-plate variation. (C) Body weight over time. Repeated-measures ANOVA, overall group effect, $P = 0.11$; n = 10–13/group. (D) Morris water maze performance at multiple time points. V1 and V2 indicate visible-platform trials 1 and 2. At 1 week, hidden-platform trials showed an overall group effect (repeated-measures ANOVA, $P = 0.0164$); Tukey's multiple-comparisons test: sham vs. TT, $P = 0.0955$; sham vs. PNAG, $P = 0.015$; TT vs. PNAG, $P = 0.7236$. The overall group effect was not significant for 1-week visible-platform trials ($P = 0.20$), 3-month hidden-platform trials ($P = 0.28$), 3-month visible-platform trials ($P = 0.14$), 6-month hidden-platform trials ($P = 0.23$), or 6-month visible-platform trials ($P = 0.08$). At 1 year, hidden-platform trials showed an overall group effect ($P = 0.0314$); Tukey's multiple-comparisons test: sham vs. TT, $P = 0.4352$; sham vs. PNAG, $P = 0.024$; TT vs. PNAG, $P = 0.3496$. The overall group effect was not significant for 1-year visible-platform trials ($P = 0.7664$). Repeated-measures ANOVA; n = 10–13/group. (E) Probe trial performance did not differ significantly among groups at any time point: 1 week, $P = 0.70$; 3 months, $P = 0.64$; 6 months, $P = 0.64$; 1 year, $P = 0.07$. One-way ANOVA; n = 10–13/group. (F) Rotarod performance showing improved motor function in PNAG-vaccinated mice. Repeated-measures ANOVA, overall group effect, $P = 0.0104$; Tukey's multiple-comparisons test: sham vs. TT, $P = 0.0133$; sham vs. PNAG, $P = 0.9235$; TT vs. PNAG, $P = 0.0317$. n = 10–13/group.

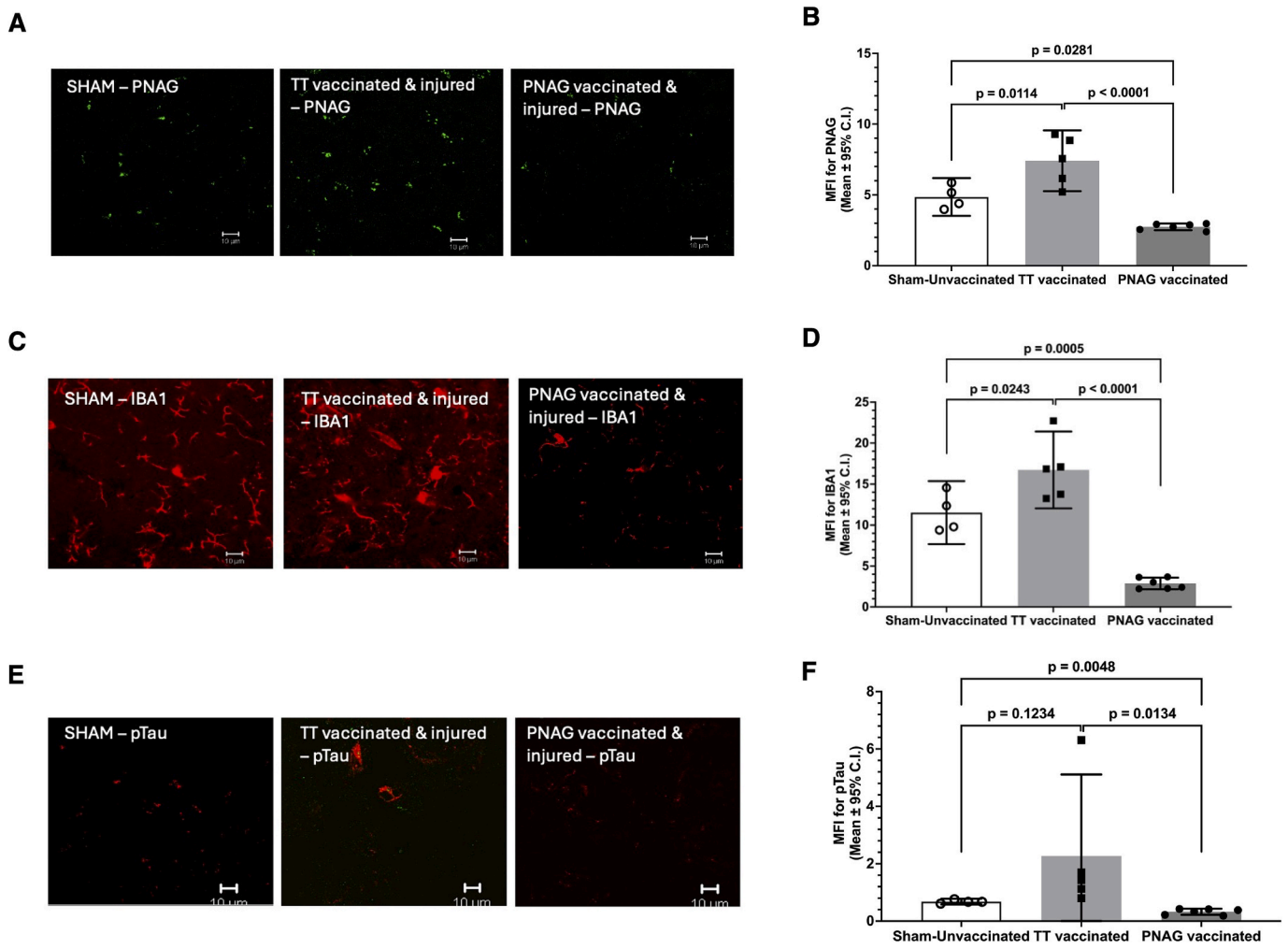


Fig. 6. PNAG vaccination reduces persistent neuropathology in striatum one year after repetitive brain injury in male mice. (A–B) PNAG immunoreactivity and quantification. Bars represent the mean of all fields analyzed from each mouse; individual symbols represent individual fields. One-way ANOVA, overall $P < 0.0001$. Tukey's multiple-comparisons test: sham vs. TT-vaccinated injured, $P = 0.0114$; sham vs. PNAG-vaccinated injured, $P = 0.0281$; TT-vaccinated injured vs. PNAG-vaccinated injured, $P < 0.0001$. (C–D) IBA1 immunoreactivity and quantification in the striatum. Bars represent the mean of all fields analyzed from each mouse; individual symbols represent individual fields. One-way ANOVA, overall $P < 0.0001$. Tukey's multiple-comparisons test: sham vs. TT-vaccinated injured, $P = 0.0243$; sham vs. PNAG-vaccinated injured, $P = 0.0005$; TT-vaccinated injured vs. PNAG-vaccinated injured, $P < 0.0001$. n = 4–6 mice/group. Scale bar, 10 μm. (E–F) pTau accumulation and quantification. Bars represent the mean of all fields analyzed from each mouse; individual symbols represent individual fields. Welch's ANOVA, overall $P = 0.0051$. Games-Howell multiple-comparisons test: sham vs. TT-vaccinated injured, $P = 0.1231$; sham vs. PNAG-vaccinated injured, $P = 0.0048$; TT-vaccinated injured vs. PNAG-vaccinated injured, $P = 0.0134$. Raw pTau MFI values were log10-transformed due to non-normal distribution; normality after transformation was confirmed by the Shapiro-Wilk test. n = 4–6 mice/group. Scale bar, 10 μm. For statistical analyses, the individual mouse was the experimental unit.

although they did not differ significantly from TT-vaccinated injured mice. This dissociation may reflect differences in the vulnerability of underlying neural circuits, the temporal dynamics of recovery, or the sensitivity of the behavioral assays. The absence of comparable cognitive benefit despite improved motor outcomes underscores the multifactorial nature of traumatic brain injury and suggests that reducing persistent microbial-derived material alone is insufficient to improve all functional domains. Traumatic brain injury initiates a complex cascade involving mechanical damage, vascular dysfunction, immune activation, and protein aggregation, and targeting a single pathway would not be expected to improve all long-term outcomes. Nutraceutical approaches have also been proposed to improve recovery following TBI through modulation of neuroinflammation, oxidative stress, mitochondrial dysfunction, and neuronal recovery (Lucke-Wold et al., 2025). Such approaches could potentially complement strategies directed at persistent microbial-derived material by targeting downstream consequences of injury through distinct or complementary mechanisms.

Sex-dependent effects were observed following intracerebral administration of purified PNAG, with male mice exhibiting motor and locomotor deficits that were less evident or not detected in females. These findings suggest that biological sex may modify the neurological response to persistent microbial-derived material. Although the present study was not designed to define the underlying mechanisms, sex-specific differences in innate immune responses, microglial biology, hormonal regulation, or the processing or clearance of microbial-derived material may contribute to these divergent outcomes. Future studies should determine the mechanisms underlying these sex-dependent responses and whether they influence susceptibility to chronic post-traumatic neuroinflammation.

Several limitations of this study should be acknowledged. Notably, several experiments, including the long-term vaccination studies, were performed only in male mice, limiting conclusions regarding whether these findings generalize to females. The human data are observational and therefore cannot establish the origin of PNAG or the route by which

it reaches the brain. In addition, intracerebral administration of purified PNAG does not fully recapitulate the complexity of microbial extracellular vesicles and other microbial-derived material that may accumulate following injury. While antibody-based approaches reduced PNAG immunoreactivity, the mechanisms underlying this reduction—whether decreased entry, enhanced clearance, altered distribution, or other processes—remain to be defined. The type and severity of brain injury may also influence these processes, as distinct injury paradigms produce different vascular, inflammatory, and gut–brain responses. Because the present study was not designed to directly compare injury paradigms, whether the entry, persistence, or effects of microbial-derived material differ among single, repetitive, focal, and more severe forms of brain injury remains to be determined. Future studies using repetitive CHI models that produce more robust and sustained cognitive deficits will be important to more fully evaluate the effects of PNAG-targeted interventions on post-traumatic cognitive outcomes. Finally, independent methods for detecting microbial-derived material, such as ELISA or mass spectrometry, will be important to further validate and extend these findings.

Despite these limitations, our findings support a conceptual framework in which persistent microbial-derived material may act as a chronic stimulus sustaining neuroinflammation following brain injury. In this model, injury-associated changes in barrier function or tissue trafficking may permit entry of microbial-derived material into the brain, where limited clearance allows it to persist. Persistent microbial-derived material may then interact with resident immune cells, sustaining inflammatory signaling and contributing to downstream pathological processes, including tau phosphorylation and functional impairment. Interventions that reduce the burden of persistent microbial-derived material may therefore attenuate chronic neuroinflammatory signaling and improve long-term neurological outcomes. A proposed mechanistic model integrating these findings is presented in the Summary Schematic.

In summary, this study identifies persistent microbial-derived material in human CTE and experimental brain injury and demonstrates that reducing this material is associated with improved neuropathological and neurological outcomes. These findings expand current models of the microbiome–brain axis by implicating persistent microbial structural components, rather than solely systemic signals, as potential contributors to post-traumatic neuroinflammation. Defining the sources, routes of entry, trafficking pathways, and immune mechanisms governing the persistence and clearance of microbial-derived material represents an important next step and may reveal new therapeutic strategies for mitigating the long-term consequences of traumatic brain injury.

4. Methods

4.1. Study overview

1. **PNAG immunohistochemistry in brains from human chronic traumatic encephalopathy (CTE) cases:** Brains (n = 10) were selected by the Boston University CTE brain bank to represent CTE stages I–IV. All cases were from males who had played soccer, rugby, or American football and had a post-mortem diagnosis of CTE. Stage I cases were ages 46, 50, and 51; stage II, ages 42 and 58; stage III, ages 41 and 49; and stage IV, ages 74, 78, and 84. Controls (n = 5) were brain samples from males aged 25, 28, 29, 35, and 45 years who had no diagnosis of CTE. The brain region analyzed was the frontal cortex.
2. **Purified PNAG treatment of human neural cells:** Differentiated human neural stem cells and induced pluripotent stem cell (iPSC)-derived neurons were treated with purified PNAG (10 μg/mL) or PBS. iPSC-derived neurons were analyzed after 1 week of PNAG exposure and neural stem cells after 2 weeks to assess tau phosphorylation.
3. **PNAG accumulation in brain after a single closed head injury (CHI):** Male mice received a single CHI or sham procedure and were euthanized at 24 h, 2 weeks, or 2 months after injury. Regional PNAG accumulation was quantified in the cortex, hippocampus, and striatum, with sham animals included for comparison. PNAG colocalization with neurons, microglia, astrocytes, and pTau was also evaluated.
4. **Effects of intrastriatal purified PNAG administration on behavioral deficits:** Male and female mice (n = 11–13/group) were administered purified PNAG or PBS bilaterally into the striatum, and behavioral outcomes were assessed for up to one week.
5. **Effects of PNAG vaccination on long-term outcomes after repetitive CHI:** Male mice (n = 10–13/group) received five weekly immunizations with PNAG vaccine or control vaccine and were subsequently subjected to sham injury or a six-hit CHI paradigm. Following injury, mice received three booster immunizations at 8-week intervals. Behavioral outcomes were assessed for up to one year, after which brains were analyzed by immunohistochemistry for PNAG and neuropathological markers.
6. **Effects of anti-PNAG monoclonal antibody treatment after repetitive CHI:** Male and female mice were studied in separate experiments in which animals were pretreated with anti-PNAG monoclonal antibody or control antibody and subjected to the seven-hit repetitive CHI (7HD) paradigm (n = 10–12/group). Behavioral outcomes were assessed for up to 7 days, followed by immunohistochemical analysis of brain PNAG accumulation.

4.2. Animals

Male and female C57BL/6J mice (2–4 months; Jackson Laboratories, Bar Harbor, ME) were used. Animals were housed under standard conditions (12-hour light/dark cycle, ad libitum food and water). All experiments were reported in accordance with the ARRIVE guidelines (Kilkenny et al., 2010) and were approved by the Massachusetts General Hospital Institutional Animal Care and Use Committee.

4.3. Closed Head Injury (CHI) Models

Closed head injury was performed as previously described with minor modifications (Wu et al., 2022; Mannix et al., 2013; Wu et al., 2019). Mice from the same cage were randomized to either sham or CHI by investigators who were not involved in administering the injuries. For the single severe CHI model, mice were anesthetized with 2.5% isoflurane in 70% nitrous oxide/30% oxygen and positioned under a vertical guide tube. A metal bolt was dropped onto the midline of the skull to induce injury. Single CHI consisted of an 81 g weight dropped from 152 cm. Repetitive 6-hit and 7-hit CHI consisted of twice-daily impacts over 3–4 days using a 54 g weight dropped from 132 cm. Impact location alternated between hemispheres for repetitive models. For the 7-HD model, a seventh injury was administered on day 4. Sham animals underwent anesthesia without impact. Latency to righting was recorded after the first injury. The single-CHI model was used to define the early time course and regional distribution of PNAG accumulation following an isolated brain injury. The 6-hit model was chosen for long-term behavioral studies to model repetitive head injury relevant to CTE, a chronic neuropathological process that develops over prolonged periods; accordingly, outcomes were assessed for up to one year. The 7HD model was chosen for short-term studies of anti-PNAG monoclonal antibody treatment in male and female mice because this injury paradigm produces robust behavioral deficits in females, which are relatively resistant to CHI-induced behavioral deficits compared with males.

4.4. PNAG purification

PNAG was purified from *S. aureus* strain MN8M as previously described (Maira-Litrán et al., 2002). Briefly, culture supernatants were

collected, ethanol-precipitated, and treated with DNase, RNase, and proteinase K. The resulting material was acid-solubilized, dialyzed, lyophilized, and confirmed to be > 99% pure by nuclear magnetic resonance spectroscopy.

4.5. Intracerebral PNAG administration

Purified PNAG (1 or 10 μg in 5 μL) or vehicle (PBS) was injected bilaterally into the striatum using stereotactic coordinates (2.0 mm lateral, 4.0 mm depth from bregma). Injections were performed over 5 min under isoflurane anesthesia.

4.6. Behavioral testing

All investigators performing behavioral testing were blinded to experimental group assignment. Mice were identified during testing only by a unique cage letter and tail mark. Group identities were revealed by investigators not involved in behavioral testing after behavioral assessments were completed, and the data were then assigned to the appropriate experimental groups for analysis.

4.7. Rotarod

Motor coordination was assessed using an accelerating rotarod (0–40 rpm over 200 s). Mice underwent three trials per session; average latency to fall was recorded.

4.8. Morris water maze

Spatial learning and memory were assessed beginning 3 days after injury or PNAG administration. Mice underwent four hidden-platform trials per day over 2 consecutive days using a submerged escape platform maintained in a fixed location. Escape latency and swim speed were recorded using automated tracking software. A probe trial was conducted 24 h after the final hidden-platform session with the platform removed to assess spatial memory retention. Visible platform testing was performed to control for visual and motor impairments.

4.9. Open field

Locomotor activity was recorded over 30 min and analyzed using automated tracking software.

4.10. Immunization and antibody treatment

4.10.1. Active vaccination

Mice received five weekly subcutaneous immunizations with PNAG conjugate vaccine (5GlcNH$_2$-TT; Alopexx, Inc., Cambridge, MA), consisting of a synthetic pentameric β-(1 → 6)-linked glucosamine oligosaccharide conjugated to tetanus toxoid (30 μg in alum) (Gening et al., 2010). Control mice received tetanus toxoid alone. Following CHI or sham injury, mice received three additional booster immunizations of the same dose at 8-week intervals. Serum anti-PNAG IgG titers were measured by enzyme-linked immunosorbent assay (Maira-Litrán et al., 2012).

4.10.2. Passive Antibody Administration

Mice received 150 μg anti-PNAG monoclonal antibody (F598) or isotype control (F429) subcutaneously 1 h prior to the first CHI (Kelly-Quintos et al., 2006).

4.11. Immunohistochemistry and Imaging

4.11.1. Murine brain sections

Mice were deeply anesthetized and transcardially perfused with PBS. Brains were post-fixed in 4% paraformaldehyde (PFA) at 4°C for 24 h, cryoprotected in 30% sucrose for two days, and frozen and stored at − 80°C. Brains were sectioned in the coronal plane at 200–300 μm intervals from anterior to posterior. Cryostat sections (12 μm) were mounted on poly-L-lysine-coated slides. For immunohistochemistry, sections were washed in PBS, blocked in 10% normal goat serum in PBS for 1 h, and incubated overnight at 4°C with rabbit anti-ionized calcium-binding adapter molecule 1 (Iba1) (1:200; Wako, Cat# 019–19741), rabbit anti-glial fibrillary acidic protein (GFAP) (1:200; Sigma, Cat# MAB3402C3), mouse anti-NeuN antibody (1:200; Millipore, Cat# MABN140), anti-phospho tau AT8 (1:500; Invitrogen, Cat# MN1020), or monoclonal anti-PNAG mAb F598 (5 μg/mL) or control mAb F429 (5 μg/mL), directly conjugated to Alexa Fluor 488 or 568 and provided by the laboratory of Dr. Gerald Pier (Kelly-Quintos et al., 2006). An Alexa Fluor 568-conjugated goat anti-rabbit secondary antibody (1:300; Invitrogen, Cat# A11011) was used for rabbit primary antibodies. Nuclei were counterstained with 4,6-diamidino-2-phenylindole (DAPI), mounted, and coverslips were secured in place. Sections were analyzed by a blinded investigator using ImageJ software (National Institutes of Health). Slides were analyzed using a Zeiss Pascal confocal microscope with the appropriate excitation/emission spectra. Brain regions assessed included the cortex, hippocampus, and striatum. For each brain region, two 63 × microscopic fields were analyzed per section from three sections per mouse (6 fields/brain region/mouse), with equal numbers of fields derived from the right and left hemispheres. Microscopic fields within each brain region were selected without reference to PNAG staining by moving the objective systematically across the tissue and randomly selecting fields for analysis. For quantitation of PNAG in mouse brains, sections were labeled with anti-PNAG F598 conjugated to Alexa Fluor 568 or Alexa Fluor 488 at 5 μg/mL. Images used for quantitative comparisons were acquired using identical microscope settings across experimental groups. PNAG immunoreactivity was quantified by mean fluorescence intensity (MFI) because staining included both diffuse and punctate signals of heterogeneous size and intensity. A control-labeled sample was used to establish the minimum fluorescence threshold for distinguishing specific signal from background, and this threshold was then applied consistently across experimental samples as the baseline for pixel-intensity measurements within the defined regions of interest. MFI was determined using ImageJ (NIH) by an investigator blinded to experimental group.

4.11.2. Human brain sections

Paraffin-embedded frontal cortex sections from five controls and ten individuals with CTE stages I–IV were obtained from the Boston University (BU) Understanding Neurologic Injury and Traumatic Encephalopathy (UNITE) Brain Bank. Sections representing the different CTE stages were selected and provided by the BU UNITE Brain Bank. Sections were deparaffinized and subjected to antigen retrieval in 10 mM citrate buffer, pH 6.0. To control for specificity of PNAG labeling, samples were pretreated with either the PNAG-specific degrading enzyme Dispersin B (Kane Biotech) or the control enzyme chitinase (Sigma) at 100 μg/mL overnight at 37°C. Samples were labeled with either control monoclonal antibody F429 or PNAG-specific monoclonal antibody F598, directly conjugated to Alexa Fluor 488 (10 μg/mL) and anti-phospho-tau antibody AT8 (Thermo Fisher; 5 μg/mL, Cat# MN1020), followed by goat anti-mouse IgG-Alexa Fluor 568 secondary antibody (Thermo Fisher; 1:500, Cat# A-11004). All samples were treated with TrueBlack (Biotium) autofluorescence quencher before imaging. Slides were imaged using a Zeiss Pascal confocal microscope with appropriate excitation and emission settings. Microscopic fields were sampled without reference to PNAG staining by moving the objective systematically across the tissue using either a 4 × 3 or 5 × 2 sampling grid, yielding 10–12 fields per section. Images used for quantitative comparisons were acquired using identical microscope settings. Mean fluorescence intensity (MFI) was determined from 63 × microscopic fields using ImageJ (NIH) by an investigator blinded to CTE stage and control status.

4.11.3. Human neural cell models

Human Induced Neural Stem Cells and iPSC-derived Neurons. Cells were cultured and differentiated as previously described (Cairns et al., 2016; Pantazis et al., 2022; Zhang et al., 2013). iPSC-derived neurons were treated with purified PNAG (10 μg/mL) or PBS for 1 week, and differentiated human neural stem cells were treated with purified PNAG (10 μg/mL) or PBS for 2 weeks.

4.11.4. Phosphorylated Tau measurement

Cell lysates were analyzed using enzyme-linked immunosorbent assays for pTau (Ser202/Thr205 and Thr181), normalized to protein content.

4.12. Statistical analysis

Data distributions were assessed for normality and appropriate parametric or non-parametric statistical tests were selected accordingly. Comparisons between two groups were performed using Student's *t*-test for normally distributed data or the Mann–Whitney test for non-parametric data. Multi-group comparisons were performed using one-way or two-way analysis of variance (ANOVA) for normally distributed data or Kruskal–Wallis analysis for non-parametric data. For datasets with unequal variances, Brown–Forsythe ANOVA followed by Dunnett's T3 multiple-comparisons testing was used. Welch's ANOVA followed by Games-Howell multiple-comparisons testing was used where indicated. Where indicated, non-normally distributed data were log10-transformed and normality after transformation was assessed using the Shapiro-Wilk test. Mixed-effects analyses were used for regional comparisons where indicated. Repeated-measures ANOVA was used for longitudinal behavioral data. Post-hoc multiple comparisons were performed using Tukey's multiple-comparisons test or the two-stage linear step-up procedure of Benjamini et al. (2006), as appropriate and as indicated in the figure legends. Statistical significance was defined as $P < 0.05$. Effect sizes were calculated as Hedges' *g* for pairwise comparisons and partial eta-squared (ηp2) for ANOVA-based analyses and are reported in Supplementary Table 1. For Hedges' *g*, 95% confidence intervals were calculated; for partial eta-squared, 90% confidence intervals were calculated as this effect size estimate cannot have a negative value so this one-sided significance test is standard. The individual animal was the experimental unit for in vivo studies, and independent biological replicates were the experimental units for in vitro studies. Data presentation and measures of variability are indicated in the corresponding figures and figure legends.

CRediT authorship contribution statement

Hongmei Yang: Writing – review & editing, Validation, Methodology, Investigation, Formal analysis, Data curation, Conceptualization. **Olivia Shyong:** Investigation, Formal analysis, Data curation. **Limin Wu:** Investigation, Formal analysis, Data curation. **Evan C. Marcet:** Writing – review & editing, Methodology, Investigation, Formal analysis, Data curation, Conceptualization. **Brianne E. Dillon:** Investigation, Formal analysis, Data curation. **Jaina T. Dillon:** Investigation, Formal analysis, Data curation. **Dalila M. Marzialo:** Investigation, Formal analysis, Data curation. **Aubrienne Krysiewicz-Bell:** Investigation, Formal analysis, Data curation. **Lindsay E. Popeo:** Investigation, Formal analysis, Data curation. **Shirin Jamali:** Investigation, Formal analysis, Data curation. **Graham Y. Schrodel:** Investigation, Formal analysis, Data curation. **Amir Davis:** Investigation, Formal analysis, Data curation. **Aria Shi:** Investigation, Formal analysis, Data curation. **Dana M. Cairns:** Investigation, Formal analysis, Data curation. **Liam H. Power:** Investigation, Formal analysis, Data curation. **David L. Kaplan:** Writing – review & editing, Supervision, Funding acquisition. **Ann McKee:** Methodology, Conceptualization. **Daniel H. Daneshvar:** Methodology, Conceptualization. **Mariana Vinacur:** Investigation, Formal analysis, Data curation. **Gerald B. Pier:** Investigation, Formal analysis, Data curation. **Ross Zafonte:** Writing – review & editing, Supervision, Methodology, Funding acquisition, Conceptualization. **Michael J. Whalen:** Writing – review & editing, Writing – original draft, Supervision, Methodology, Investigation, Funding acquisition, Formal analysis, Data curation, Conceptualization. **Colette Cywes-Bentley:** Writing – review & editing, Writing – original draft, Visualization, Validation, Supervision, Resources, Project administration, Methodology, Investigation, Funding acquisition, Formal analysis, Data curation, Conceptualization.

Funding

This work was supported by the National Football League Players Association (NFLPA) grant to Harvard College (CC-B, MJW, RZ); the Department of Defense [W81XWH-19-2-0276] (CC-B and MJW); The Gillian Reny Stepping Strong Center for Trauma Innovation Innovator Award (CC-B and MJW); and the Department of Defense Multiple University Research Initiative (MURI) [W911NF-23-1-0276] (CC-B, MJW, DLK, and DMC). GlcNH2-TT vaccine AV0328 and monoclonal antibody F598 were provided by Alopexx, Inc. (Cambridge, MA). CTE tissue was obtained from the BU ADRC and BU CTE Center funded by the NIH P30AG072978, U01NS086659, and U54NS115266.

Declaration of competing interest

The authors declare the following financial interests/personal relationships which may be considered as potential competing interests: Gerald B. Pier and Colette Cywes-Bentley have a financial interest in Alopexx, a company developing broad-spectrum immune therapeutics, which target the polysaccharide, poly *N*-acetyl glucosamine (PNAG) for the prevention, treatment, and mitigation of bacterial, fungal, and parasitic infections. Drs. Pier and Cywes-Bentley's interests were reviewed and are managed by Mass General Brigham in accordance with their conflict-of-interest policies.

Appendix A. Supplementary data

Supplementary data to this article can be found online at https://doi.org/10.1016/j.bbi.2026.107082. Supplementary figures and table providing additional experimental data on PNAG-associated neuropathology, behavioral outcomes following anti-PNAG antibody treatment, and statistical effect sizes.

Data availability

Data will be made available on request.

References

Benjamini, Y., Krieger, A.M., Yekutieli, D., 2006. Adaptive linear step-up procedures that control the false discovery rate. Biometrika 93, 491–507.

Bieniek, K.F., Cairns, N.J., Crary, J.F., Dickson, D.W., Folkerth, R.D., Keene, C.D., et al., 2021. TBI/CTE Research Group. The second NINDS/NIBIB consensus meeting to define neuropathological criteria for the diagnosis of chronic traumatic encephalopathy. J. Neuropathol. Exp. Neurol. 80 (3), 210–219. https://doi.org/10.1093/jnen/nlab001.

Brett, B.L., Gardner, R.C., Godbout, J., Dams-O'Connor, K., Keene, C.D., 2022. Traumatic brain injury and risk of neurodegenerative disorder. Biol. Psychiatry 91 (5), 498–507. https://doi.org/10.1016/j.biopsych.2021.05.025.

Cairns, D.M., Chwalek, K., Moore, Y.E., Kelley, M.R., Abbott, R.D., Moss, S., Kaplan, D.L., 2016. Expandable and rapidly differentiating human induced neural stem cell lines for multiple tissue engineering applications. Stem Cell Rep. 7 (3), 557–570. https://doi.org/10.1016/j.stemcr.2016.07.017.

Cywes-Bentley, C., Skurnik, D., Zaidi, T., Roux, D., Deoliveira, R.B., Garrett, W.S., et al., 2013. Antibody to a conserved antigenic target is protective against diverse prokaryotic and eukaryotic pathogens. PNAS 110 (24), E2209–E2218. https://doi.org/10.1073/pnas.1303573110.

Gening, M.L., Maira-Litrán, T., Kropec, A., Skurnik, D., Grout, M., Tsvetkov, Y.E., Nifantiev, N.E., Pier, G.B., 2010. Synthetic {beta}-(1->6)-linked N-acetylated and nonacetylated oligoglucosamines used to produce conjugate vaccines for bacterial pathogens. Infect. Immun. 78 (2), 764–772. https://doi.org/10.1128/IAI.01093-09.

Gening, M.L., Pier, G.B., Nifantiev, N.E., 2020. Broadly protective semi-synthetic glycoconjugate vaccine against pathogens capable of producing poly-β-(1→6)-N-acetyl-D-glucosamine exopolysaccharide. Drug Discov. Today Technol. 35–36, 13–21. https://doi.org/10.1016/j.ddtec.2020.09.002.

Gu, N., Yan, J., Tang, W., Zhang, Z., Wang, L., Li, Z., et al., 2024. Prevotella copri transplantation promotes neurorehabilitation in a mouse model of traumatic brain injury. J. Neuroinflammation 21 (1), 147. https://doi.org/10.1186/s12974-024-03116-5.

Kelly-Quintos, C., Cavacini, L.A., Posner, M.R., Goldmann, D., Pier, G.B., 2006. Characterization of the opsonic and protective activity against *S. aureus* of fully human monoclonal antibodies specific for the bacterial surface polysaccharide poly-N-acetylglucosamine. Infect. Immun. 74 (5), 2742–2750. https://doi.org/10.1128/IAI.74.5.2742-2750.2006.

Kilkenny, C., Browne, W.J., Cuthill, I.C., Emerson, M., Altman, D.G., 2010. Improving bioscience research reporting: the ARRIVE guidelines for reporting animal research. PLoS Biol. 8 (6), e1000412. https://doi.org/10.1371/journal.pbio.1000412.

Kim, O.Y., Park, H.T., Dinh, N.T.H., Choi, S.J., Lee, J., Kim, J.H., et al., 2017. Bacterial outer membrane vesicles suppress tumor by interferon-γ-mediated antitumor response. Nat. Commun. 8 (1), 626. https://doi.org/10.1038/s41467-017-00729-8.

Lucke-Wold, B., Zasler, N.D., Ruchika, F., Weisman, S., Le, D., Brunicardi, J., et al., 2025. Supplement and nutraceutical therapy in traumatic brain injury. Nutr. Neurosci. 28 (6), 709–743. https://doi.org/10.1080/1028415X.2024.2404782.

Maira-Litrán, T., Bentancor, L.V., Bozkurt-Guzel, C., O'Malley, J.M., Cywes-Bentley, C., Pier, G.B., 2012. Synthesis and evaluation of a conjugate vaccine composed of *S. aureus* poly-N-acetyl-glucosamine and clumping factor a. PLoS One 7 (9), e43813. https://doi.org/10.1371/journal.pone.0043813.

Maira-Litrán, T., Kropec, A., Abeygunawardana, C., Joyce, J., Mark 3rd, G., Goldmann, D.A., Pier, G.B., 2002. Immunochemical properties of the staphylococcal poly-N-acetylglucosamine surface polysaccharide. Infect. Immun. 70 (8), 4433–4440. https://doi.org/10.1128/IAI.70.8.4433-4440.2002.

Maira-Litrán, T., Kropec, A., Goldmann, D.A., Pier, G.B., 2005. Comparative opsonic and protective activities of *S. aureus* conjugate vaccines containing native or deacetylated Staphylococcal Poly-N-acetyl-beta-(1-6)-glucosamine. Infect. Immun. 73 (10), 6752–6762. https://doi.org/10.1128/IAI.73.10.6752-6762.2005. Erratum. In: Infect Immun. 2005 Nov; 73(11):7789.

Mannix, R., Meehan, W.P., Mandeville, J., Grant, P.E., Gray, T., Berglass, J., et al., 2013. Clinical correlates in an experimental model of repetitive mild brain injury. Ann. Neurol. 74 (1), 65–75. https://doi.org/10.1002/ana.23858.

Oyovwi, M.O., Udi, O.A., 2025. The gut-brain axis and neuroinflammation in traumatic brain injury. Mol. Neurobiol. 62 (4), 4576–4590. https://doi.org/10.1007/s12035-024-04585-8.

Pantazis, C.B., Yang, A., Lara, E., McDonough, J.A., Blauwendraat, C., Peng, L., et al., 2022. A reference human induced pluripotent stem cell line for large-scale collaborative studies. Cell Stem Cell 29 (12), 1685–1702.e22. https://doi.org/10.1016/j.stem.2022.11.004.

Panther, E.J., Dodd, W., Clark, A., Lucke-Wold, B., 2022. Gastrointestinal microbiome and neurologic injury. Biomedicines 10 (2), 500. https://doi.org/10.3390/biomedicines10020500.

Shumilov, K., Ni, A., Garcia-Bonilla, M., Celorrio, M., Friess, S.H., 2024. Early depletion of gut microbiota shape oligodendrocyte response after traumatic brain injury. J. Neuroinflammation 21 (1), 171. https://doi.org/10.1186/s12974-024-03158-9.

Wu, L., Chung, J.Y., Saith, S., Tozzi, L., Buckley, E.M., Sanders, B., et al., 2019. Repetitive head injury in adolescent mice: a role for vascular inflammation. J. Cereb. Blood Flow Metab. 39 (11), 2196–2209. https://doi.org/10.1177/0271678X18786633.

Wu, L., Kalish, B.T., Finander, B., Cao, T., Jin, G., Yahya, T., et al., 2022. Repetitive mild closed head injury in adolescent mice is associated with impaired proteostasis, neuroinflammation, and tauopathy. J. Neurosci. 42 (12), 2418–2432. https://doi.org/10.1523/JNEUROSCI.0682-21.2021.

Yuan, B., Lu, X.J., Wu, Q., 2021 Dec. Gut microbiota and acute central nervous system injury: a new target for therapeutic intervention. Front. Immunol. 24 (12), 800796. https://doi.org/10.3389/fimmu.2021.800796.

Zhang, Y., Pak, C., Han, Y., Ahlenius, H., Zhang, Z., Chanda, S., et al., 2013. Rapid single-step induction of functional neurons from human pluripotent stem cells. Neuron 78 (5), 785–798. https://doi.org/10.1016/j.neuron.2013.05.029.